Electron acceleration due to small pulses in shock waves in inhomogeneous plasmas: Perpendicular propagation

Masatoshi Sato and Yukiharu Ohsawa[a)]
Department of Physics, Nagoya University, Nagoya 464-8602, Japan

(Received 28 February 2006; accepted 2 June 2006; published online 30 June 2006)

Electron acceleration in shock waves propagating perpendicular to an external magnetic field, which is inhomogeneous and reversed in a finite region, is studied with relativistic particle simulations. By the time a shock wave reaches the inhomogeneous region, some electrons are energized by a small compressive pulse generated in the shock wave. After penetrating this region, the original shock wave is damped. However, a new shock wave with the magnetic polarity opposite to that of the original shock wave is excited. In this secondary shock wave, particle-accelerating compressive pulses are also generated. Further, after the encounter with the original shock wave, the magnetic null point starts to move with a slightly slower speed than the secondary shock wave, and electric fields are formed around it. Some electrons also gain energy in meandering orbits around the field-reversed pulse. © *2006 American Institute of Physics*. [DOI: 10.1063/1.2217709]

I. INTRODUCTION

Electron acceleration to ultrarelativistic energies has been observed in many astrophysical and laboratory plasmas. For example, electrons can be promptly accelerated to several tens of MeV in solar flares.[1–3] Shock waves of supernova remnants can produce electrons with energies $\sim 10^{14}$ eV.[4–7] Laboratory experiments of plasma-based accelerators[8,9] have demonstrated electron energization to a few hundred MeV with a short acceleration gradient ~ 200 GeV/m.[10]

In addition, particle simulations have shown that a shock wave propagating obliquely to an external magnetic field can promptly accelerate electrons to ultrarelativistic energies such that $\gamma > 100$, where γ is the Lorentz factor.[11] Some electrons are reflected in the end of the main pulse region of the shock wave. They are then trapped and energized in the wave. This acceleration occurs in rather strong magnetic fields such that $|\Omega_e|/\omega_{pe} \gtrsim 1$ and is particularly strong when the shock propagation speed v_{sh} is close to $c\cos\theta$, where Ω_e (<0) is the nonrelativistic electron gyrofrequency, ω_{pe} is the plasma frequency, c is the speed of light, and θ is the angle between the wave normal and the external magnetic field.

Quite recently, simulations of electron acceleration to $\gamma \sim 100$ with a different mechanism have been reported.[12] Usually, propagation of a large-amplitude shock wave is not perfectly stationary,[11–14] even though we know solutions showing stationary propagation of small-amplitude waves.[15–19] Fluctuations are present in shock waves even in the absence of current-driven instabilities. It has been shown that some of the small-amplitude compressive pulses generated in shock waves can cause energization of electrons. These electrons gain energy from the transverse electric fields immediately behind the pulses. An important point in this process is that electric fields exist outside the small pulses as well as inside them because the pulses are in shock waves (behind the shock transition region). In the simulations of Ref. 12, compressive small pulses around which the electron acceleration takes place are generated in association with ion reflection by a shock wave.[14] That is, the sharp rise of electric potential and magnetic field in a shock wave can give rise to the ion reflection,[20–26] which then affects the evolution of the wave profile. Since the propagation speeds of these pulses are slightly slower than that of the main pulse, the acceleration region gradually moves backwards relative to the main pulse. This acceleration mechanism can operate in weak magnetic fields such that $|\Omega_e|/\omega_{pe} < 1$ as well as in strong magnetic fields. In addition, it does not require the condition $v_{sh} \sim c\cos\theta$.

In those simulations, small pulses that accelerated electrons were not many, usually only one in one shock wave, even though fluctuations were always present. It is therefore important to seek circumstances where particle-accelerating small pulses are generated in a shock wave. It is expected that waves would become highly nonstationary and produce a larger number of small pulses if the wave amplitude is increased or if inhomogeneity of the background plasma is introduced. In this paper, we investigate the latter case; the effect of inhomogeneity of the background plasma on the generation of particle-accelerating small pulses.

In Sec. II, we outline the acceleration mechanism due to a small pulse in a shock wave. We consider two typical motions; gyro and meandering orbits. The former, which was studied in Ref. 12, occurs around a compressive pulse where the magnetic field is stronger than that outside of it. Some electrons perform large-radius gyromotions many times around the back slope of the compressive small pulse; in the momentum space, their orbits are ellipse-like. Since the particle absorbs energy from the transverse electric field behind the pulse, the particle energy grows during the gyromotions. The latter, meandering orbit, occurs in a field-reversed small pulse; if the magnetic polarity changes across a certain line, some particles exhibit meandering motions along the line of

[a)]Electronic mail: ohsawa@nagoya-u.jp

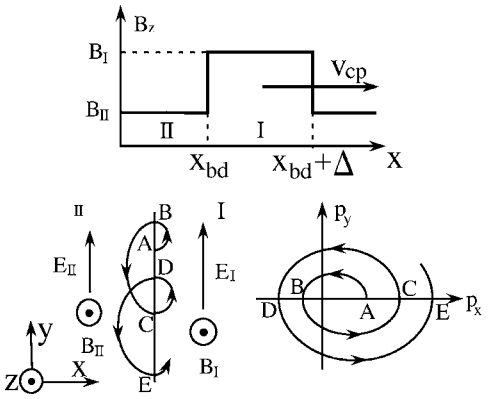

FIG. 1. Schematic diagram of compressive small pulse ($B_I B_{II} > 0$) and electron orbits in the (x,y) and (p_x,p_y) planes. The orbit in the momentum space is ellipse-like.

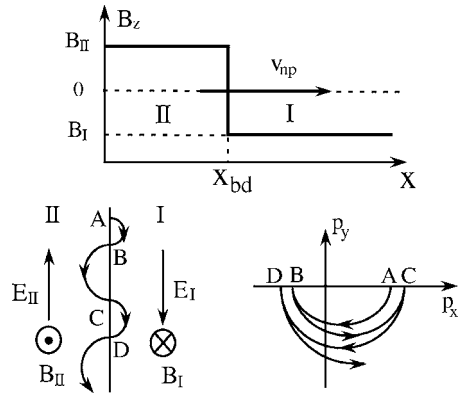

FIG. 2. Schematic diagram of field-reversed small pulse ($B_I B_{II} < 0$) and electron orbits in the (x,y) and (p_x,p_y) planes. The particle exhibits a meandering orbit in the coordinate space.

the field reversal and can gain energy from the transverse electric field. It is important to note here again that, owing to the shock wave, electric fields exist around the line of the field reversal.

In Sec. III, we use a one-dimensional (one space coordinate and three velocities), relativistic, electromagnetic particle simulation code to study the effect of inhomogeneity of the external magnetic field and plasma density. Shock waves propagate in the direction perpendicular to the external magnetic field that is reversed across a certain point. It is found that the inhomogeneity of the background plasma enhances the generation of small pulses that can accelerate electrons. That is, before a shock wave reaches the inhomogeneous region, energy multiplication of electrons can take place around a compressive small pulse in the shock wave, as in the simulations in Ref. 12. After the original shock wave penetrates the inhomogeneous region, it is gradually damped, and a secondary shock wave is formed in the region of the reversed external magnetic field; the magnetic-field direction of the secondary shock wave is thus opposite to that of the original one. The secondary shock wave also produces compressive small pulses, and they can accelerate electrons. In addition, because electric fields are generated around the magnetic null point, which starts to move with a speed slightly slower than the secondary shock wave, some electrons gain energies in the meandering motions around this field-reversed pulse. We thus have two types of particle-accelerating small pulses. We summarize our work in Sec. IV.

II. ELECTRON ORBITS CROSSING A DISCONTINUITY

We consider particle orbits with gyroradii much greater than the scale length of field variations. In the analysis, we thus assume for simplicity that the field profiles of small pulses are rectangular.[12] The magnetic field is supposed to be in the z direction, and the fields vary with x. We discuss electron motions crossing a boundary at $x=x_{bd}$ between regions I ($x>x_{bd}$) and II ($x<x_{bd}$). In the case of Fig. 1, region I ($x_{bd}<x<x_{bd}+\Delta$) represents the region of a compressive small pulse, which moves with a constant velocity v_{cp}. In each region, the electric and magnetic fields are taken to be

$$\boldsymbol{E}_\lambda = (0, E_\lambda, 0), \tag{1}$$

$$\boldsymbol{B}_\lambda = (0, 0, B_\lambda), \tag{2}$$

where the subscript λ denotes region I or II, and E_λ and B_λ have the same sign. In each region, a particle moves in an ellipse in the momentum space,

$$\frac{(p_x - P_\lambda)^2}{a_\lambda^2} + \frac{p_y^2}{(a_\lambda/\gamma_{d\lambda})^2} = 1, \tag{3}$$

where $\gamma_{d\lambda} = (1 - v_{d\lambda}^2/c^2)^{-1/2}$ with

$$v_{d\lambda} = cE_\lambda/B_\lambda, \tag{4}$$

and P_λ and a_λ are defined as

$$P_\lambda = m_e \gamma_{d\lambda}^2 v_{d\lambda} \gamma_{0\lambda} (1 - v_{d\lambda} v_{x0\lambda}/c^2), \tag{5}$$

$$a_\lambda^2 = (c^2/v_{d\lambda}^2) P_\lambda^2 - (m_e^2 c^2 + p_z^2) \gamma_{d\lambda}^2. \tag{6}$$

Here, $v_{x0\lambda}$ and $\gamma_{0\lambda}$ are the initial values of the velocity component v_x and Lorentz factor γ, respectively; we have chosen the initial value of v_y to be zero. It is proved that $P_\lambda > 0$ and that $a_\lambda^2 \geq 0$.[12] If v_{cp} is close to $v_{d\lambda}$, then particles can stay around the boundary for long periods of time.

This analysis is also applicable to the field-reversed small pulse where $B_I B_{II} < 0$, even though the particle orbit is quite different from the one in Fig. 1. As shown in Fig. 2, particles can exhibit meandering motions along the line of the magnetic null in this case.

We discuss the two types of electron motions separately.

A. Growing ellipse in momentum space

As shown in Fig. 1, the ellipse in the momentum space can become larger with time for a compressive small pulse. This can occur under the conditions that

$$B_I > B_{II} > 0, \tag{7}$$

and

$$\frac{E_{\mathrm{II}}}{B_{\mathrm{II}}} > \frac{E_{\mathrm{I}}}{B_{\mathrm{I}}} > 0. \tag{8}$$

Because the gyroradius in region II is greater than that in region I, the guiding center slowly moves in the negative y direction. The particle loses energy in region I, whereas it gains energy in region II. Under the second condition, (8), the net energy increases. The radius of the ellipse in the momentum space grows as the particle crosses the boundary $x=x_{\mathrm{bd}}$. This is the process analyzed in detail in Ref. 12. Region I corresponds to the small-pulse region in a shock wave. We note that it was also shown there that

$$v_{\mathrm{cp}} < v_{d\mathrm{I}} < v_{d\mathrm{II}} < v_{\mathrm{sh}}, \tag{9}$$

for such a case, where v_{sh} is the shock speed.

By connecting the orbits (3) inside and behind the compressive small pulse, we obtain the Lorentz factor γ at point C in terms of γ at point B (for points B and C, see Fig. 1). When $\gamma \gg 1$, we have[12]

$$\gamma(\mathrm{C}) = \frac{1+E_{\mathrm{II}}/B_{\mathrm{II}}}{1-E_{\mathrm{II}}/B_{\mathrm{II}}}\gamma(\mathrm{B}). \tag{10}$$

In addition, the energy increase from points A to C is given as

$$\gamma(\mathrm{C}) - \gamma(\mathrm{A}) = \left[\left(\frac{1+E_{\mathrm{II}}/B_{\mathrm{II}}}{1-E_{\mathrm{II}}/B_{\mathrm{II}}}\right)\left(\frac{1-E_{\mathrm{I}}/B_{\mathrm{I}}}{1+E_{\mathrm{I}}/B_{\mathrm{I}}}\right) - 1\right]\gamma(\mathrm{A}). \tag{11}$$

Equation (10) indicates that the energy multiplication is particularly enhanced when $E_{\mathrm{II}}/B_{\mathrm{II}} \sim 1$. The time rate of change averaged over a cycle is

$$\frac{d\gamma}{dt} = \frac{2|\Omega_{e\mathrm{II}}|}{\pi}\frac{(E_{\mathrm{II}}/B_{\mathrm{II}} - E_{\mathrm{I}}/B_{\mathrm{I}})}{[\gamma_{d\mathrm{II}}(1-E_{\mathrm{I}}/B_{\mathrm{I}}) + \gamma_{d\mathrm{I}}(B_{\mathrm{II}}/B_{\mathrm{I}})(1-E_{\mathrm{II}}/B_{\mathrm{II}})]}, \tag{12}$$

where $\Omega_{e\mathrm{II}}$ (<0) is the nonrelativistic electron gyrofrequency in region II. These relations are valid even when the external magnetic field has the x component, if the change in p_z is small.[12]

B. Meandering orbit

The meandering orbit in the coordinate space can occur when the field is reversed across the boundary

$$B_{\mathrm{I}} < 0 < B_{\mathrm{II}} \tag{13}$$

(see Fig. 2). This type of magnetic profile will be realized if a shock wave crosses a magnetic neutral sheet.[27–31] Collisions of two magnetic tubes could also result in this situation.[32,33] The magnetic field geometry can be quite similar to that of the Harris equilibrium.[27] Because of the shock wave, however, the transverse electric field E_y exists in regions I and II. Since E_y and B_z have similar profiles, E_y/B_z is also positive in this case.

As shown in the lower panel of Fig. 2, some electrons can continue to move in the negative y direction in this geometry. They absorb energy in region II, and the net energy gain is positive if $v_{d\mathrm{II}} > v_{d\mathrm{I}}$. Calculations similar to those in Ref. 12 show that Eqs. (10)–(12) are also applicable in this case to particles crossing the boundary at nearly right angles.

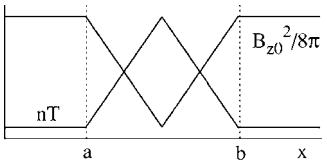

FIG. 3. Initial profiles of magnetic and plasma pressures in the upstream region.

The particle motion in the momentum space is also quite different from that in Fig. 1. It is a semi-elliptic orbit in the lower half-plane.

The propagation speed of the magnetic null point (v_{np}) is between $v_{d\mathrm{I}}$ and $v_{d\mathrm{II}}$. That is, from Faraday's law, we find that either the relation

$$v_{d\mathrm{I}} < v_{\mathrm{np}} < v_{d\mathrm{II}}, \tag{14}$$

or

$$v_{d\mathrm{I}} > v_{\mathrm{np}} > v_{d\mathrm{II}}, \tag{15}$$

holds for nearly steady propagation. The kinetic energy increases in the former. If there is a compressive small pulse in front of the null point, then by virtue of Eqs. (9) and (14), we obtain the following relation:

$$v_{\mathrm{cp}} < v_{\mathrm{np}} < v_{\mathrm{sh}}. \tag{16}$$

The speed of the field-reversed pulse (v_{np}) satisfying (14) should be greater than that of the compressive small pulse.

III. SIMULATIONS OF SHOCK WAVES IN INHOMOGENEOUS MAGNETIC FIELDS

A. Simulation model

We use a one-dimensional (one space coordinate and three velocities), relativistic, electromagnetic particle simulation code with full ion and electron dynamics[34] to study shock waves and particle acceleration. The method of simulations of shock waves is described in Refs. 11 and 24.

Shock waves propagate in the positive x direction in an external magnetic field $B_{z0}(x)$. Schematic profiles of B_{z0}^2 and plasma pressure nT in the upstream region at $t=0$ are depicted in Fig. 3. Initially, the equilibrium condition is satisfied in the upstream region,

$$\frac{B_{z0}(x)^2}{8\pi} + n(x)T = \mathrm{const}, \tag{17}$$

where the temperature T is constant. We take the profile of B_{z0} in the inhomogeneous region $a<x<b$, where a and b are constant, to be

$$B_{z0}(x) = \pm B_{z0}(a)\left|1 - \frac{2(x-a)}{b-a}\right|^{1/2}. \tag{18}$$

Here, we use the upper (+) and lower (−) signs for the regions $a<x<(a+b)/2$ and $(a+b)/2<x<b$, respectively; the field is reversed across the point $x=(a+b)/2$. The magnetic field $B_{z0}(x)$ is constant outside these regions; i.e., $B_{z0}(x)$

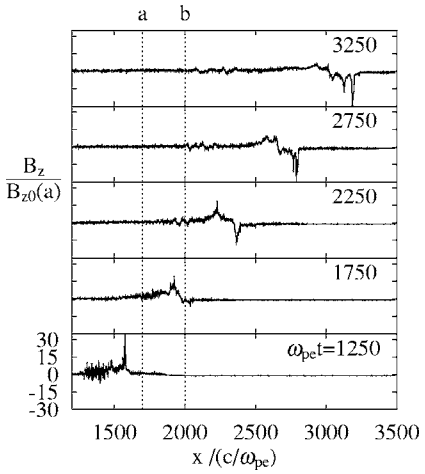

FIG. 4. Magnetic field profiles at various times. The external magnetic field B_{z0} varies with x in the region $a<x<b$ from $B_{z0}(a)$ to $B_{z0}(b)=-B_{z0}(a)$, where $a/(c/\omega_{pe})=1700$ and $b/(c/\omega_{pe})=2000$.

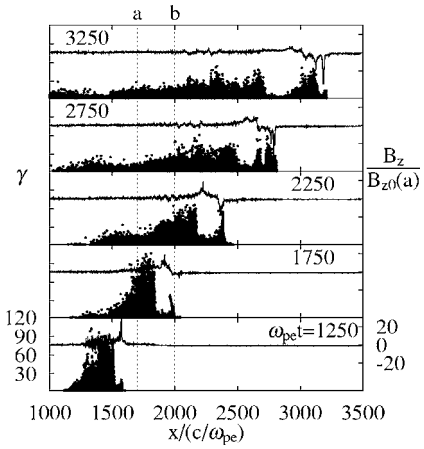

FIG. 5. Phase space plots (x,γ) of electrons and B_z profiles. The secondary shock wave as well as the original one produces high-energy electrons.

$=B_{z0}(a)>0$ for $x\leq a$, and $B_{z0}(x)=-B_{z0}(a)$ for $x\geq b$. The inhomogeneity length $(b-a)$ is chosen to be longer than the width of the shock transition region. We will observe the propagation of shock waves in this type of nonuniform external magnetic field. We are particularly interested in the wave evolution and electron acceleration after the penetration of the original shock wave into the inhomogeneous region.

The simulation parameters are as follows. The total system length is $L=16\,384\Delta_g$, where Δ_g is the grid spacing. The numbers of simulation particles are $N_i=N_e\simeq 1.05\times 10^6$. The ion-to-electron mass ratio is $m_i/m_e=100$. The speed of light is $c/(\omega_{pe}\Delta_g)=4$, where ω_{pe} is the electron plasma frequency calculated by use of the electron density averaged over the entire plasma region. The electron gyrofrequency is $|\Omega_e|/\omega_{pe}=0.4$ for the magnetic field strength $B_{z0}(a)$; hence, the Alfvén speed is $v_A/(\omega_{pe}\Delta_g)=0.16$. The thermal speeds are $v_{T_i}/(\omega_{pe}\Delta_g)=0.1$ and $v_{T_e}/(\omega_{pe}\Delta_g)=1.0$; thus, the sound speed is $c_s/(\omega_{pe}\Delta_g)=0.18$ for the specific heat ratio $\gamma_e=\gamma_i=5/3$. The speed of the linear magnetosonic wave is $v_{ms}/(\omega_{pe}\Delta_g)=0.24$, where v_{ms} is defined by $v_{ms}=(v_A^2+c_s^2)^{1/2}$. The time step is $\omega_{pe}\Delta t=0.05$.

B. Simulation results

Figure 4 displays the profiles of B_z at various times. Here, a and b are taken to be $a/(c/\omega_{pe})=1700$ and $b/(c/\omega_{pe})=2000$; these positions are indicated by the dotted vertical lines. At $\omega_{pe}t=1250$, a shock wave, which propagates with a speed $13.8v_{ms}$, is in the region $x<a$ and thus has positive B_z. At $\omega_{pe}t=1750$, it is in the nonuniform-B_{z0} region. At $\omega_{pe}t=2250$, two large pulses are present; one with positive B_z and the other with negative B_z. The former, which is the original shock wave, is gradually damped in the region of negative B_{z0}. The latter is created from the strong disturbance arising from the penetration of the original shock wave into the nonuniform-B_{z0} region. This pulse quickly evolves into an ordinary magnetosonic shock wave. At $\omega_{pe}t=3250$, this secondary shock wave is dominant. For $\omega_{pe}t\gtrsim 2250$, it propagates with a speed $v_{sh}=13.5v_{ms}$.

Figure 5 displays phase space plots (x,γ) of electrons; B_z profiles are also plotted. As shown by the picture at $\omega_{pe}t=1250$, by the time the original shock wave enters the nonuniform-B_{z0} region, some electrons have been accelerated to high energies. This acceleration mechanism is the same as the one studied in Ref. 12; i.e., the energization caused by a compressive small pulse generated in a shock wave. In the study in Ref. 12, where the external magnetic field B_{z0} was uniform, such a small pulse was generated only once in a simulation run. In the present simulation, however, ultrarelativistic electrons are also produced in the secondary shock wave; for instance, at $\omega_{pe}t=3250$, ultrarelativistic electrons are present near the points $x/(c/\omega_{pe})=3030$ and $x/(c/\omega_{pe})=3100$. Across the former point, B_z is reversed.

Figure 6 shows the trajectories of the two shock waves, and compressive and field-reversed small pulses. The original shock wave, which is represented by the closed squares, is damped after penetrating the inhomogeneous region $(a<x<b)$ at $\omega_{pe}t=1375$. In addition, the compressive small

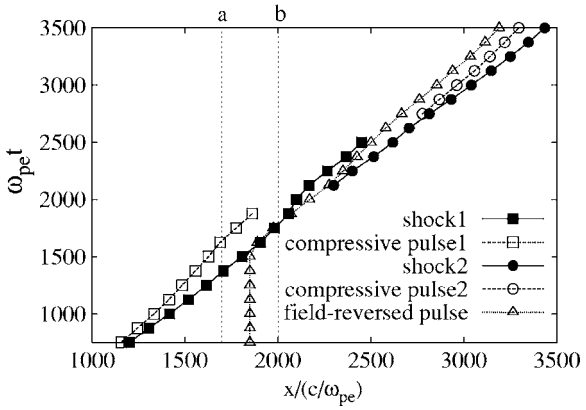

FIG. 6. Characteristics of the original shock wave (closed squares), compressive small pulse in the original shock wave (open squares), secondary shock wave (closed circles), and compressive (open circles) and field-reversed (open triangles) small pulses in the secondary shock wave.

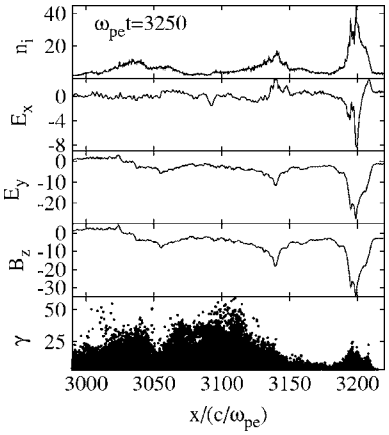

FIG. 7. Expanded view of ion density, fields, and electron phase space (x,γ). At this moment, the main pulse is at $x/(c/\omega_{pe})\simeq 3200$, a particle-accelerating compressive small pulse is at $x/(c/\omega_{pe})\simeq 3140$, and the field-reversed pulse is at $x/(c/\omega_{pe})\simeq 3030$.

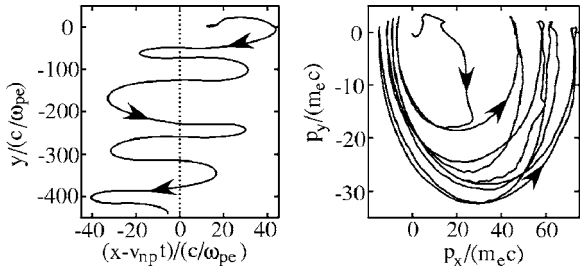

FIG. 8. Orbits of an accelerated electron in the $(x-v_{\rm np}t,y)$ and (p_x,p_y) planes. The dotted vertical line in the left panel indicates the magnetic null point.

pulse (open squares) generated in the original shock wave disappears. The secondary shock wave (closed circles) is then formed. In addition, a compressive small pulse (open circles) is generated in it, propagating with a speed $v_{\rm cp}=10.5v_{\rm ms}$. In addition, the magnetic null point (open triangles) starts to move in the positive x direction when it encounters the original shock wave. The speed of this field-reversed pulse is $v_{\rm np}=11.9v_{\rm ms}$ for $2500<\omega_{pe}t<3250$. It is slower than the shock speed $v_{\rm sh}=13.5v_{\rm ms}$ and is faster than the speed of the compressive small pulse: $v_{\rm cp}=10.5v_{\rm ms}$. This relation is consistent with Eq. (16).

Figure 7 shows an expanded view of the field profiles and phase space (x,γ) at $\omega_{pe}t=3250$. Here, the density and fields are normalized to the initial average density in $x>b$ and to the magnetic field $B_{z0}(a)$, respectively. As in ordinary magnetosonic waves,[11,15–19] B_z and E_y have similar profiles. The main pulse is at $x/(c/\omega_{pe})\simeq 3200$ at this moment. The particle-accelerating compressive small pulse, which was represented by the open circles in Fig. 6, exists at $x/(c/\omega_{pe})\simeq 3140$, behind which we find ultrarelativistic electrons. The fields B_z and E_y are reversed across the point $x/(c/\omega_{pe})\simeq 3030$, and high-energy electrons are present around this point; i.e., in $3000\lesssim x/(c/\omega_{pe})\lesssim 3050$. The maximum values of γ near the compressive and field-reversed pulses are both ~ 60 in this example. In addition, as shown in the top panel of Fig. 5, the maximum γ in the original shock wave is about 60 at this time.

Because the energization mechanism behind a compressive small pulse has been investigated in detail in Ref. 12, we here focus on the electron acceleration occurring around the field-reversed pulse. Figure 8 shows the orbit of an accelerated electron in the $(x-v_{\rm np}t,y)$ plane and that in the (p_x,p_y) plane. The dotted vertical line in the left panel indicates the null point. The particle moves in the negative y direction, crossing this line many times. In the momentum space, the particle sharply changes its direction at $p_y\simeq 0$ and exhibits semi-elliptic orbit with its radius growing with time. These trajectories in the coordinate and momentum spaces are analogous to those of the meandering particles illustrated in Sec. II.

This type of particle acceleration around the null point does not occur in the absence of shock waves. We find no high-energy electrons near the null point before the arrival of the original shock wave; see the phase space plot at $\omega_{pe}t=1250$ in Fig. 5.

The time variation of γ of this particle is depicted in the bottom panel of Fig. 9. The middle panel shows $B_z[x(t)]$ at the positions of this particle. The top panel shows the work done by the electric field,

$$W_\sigma=-e\int E_\sigma v_\sigma dt, \tag{19}$$

where the subscript σ denotes x, y, or z. Because $E_z=0$ in the present geometry, $W_z=0$. The behavior of W_y resembles that of γ, indicating that this particle absorbs energy mainly from E_y. The magnetic field is negative, for instance, from times A to B and is positive from times B to C (compare with Fig. 2). Both γ and W_y go up when the particle is in the region of positive B_z, which is in accord with the description in Sec. II B.

The predicted and simulation values of energy increase $\delta\gamma$ are of the same order of magnitude. For instance, from times B to C in Fig. 9, $\delta\gamma$ is 47.7. For the same period, Eq. (10) gives $\delta\gamma=44.7$, where for $E_{\rm II}$ and $B_{\rm II}$ we have used the average values observed in the simulation,

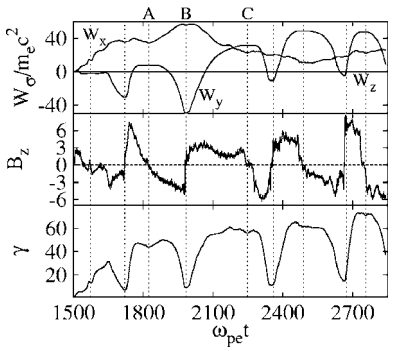

FIG. 9. Time variations of W_σ, B_z, and γ of an accelerated electron.

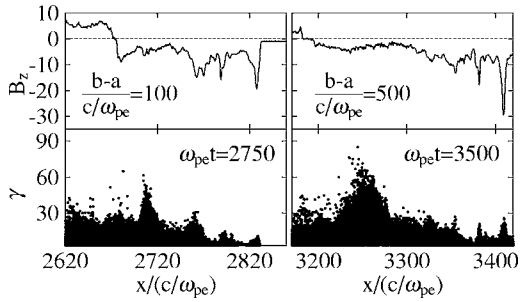

FIG. 10. Magnetic field profiles and electron phase space plots (x,γ) for shorter and longer inhomogeneity lengths $(b-a)$. In the left panels for $(b-a)/(c/\omega_{pe})=100$, high-energy electrons are found around compressive and field-reversed small pulses. In the right panels for $(b-a)/(c/\omega_{pe})=500$, acceleration behind compressive pulses is more significant.

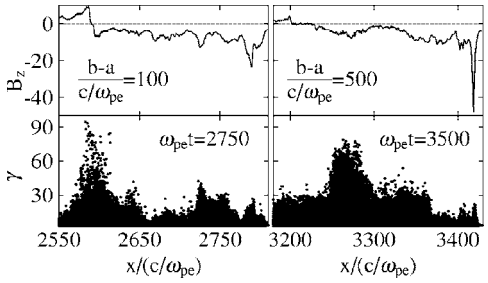

FIG. 11. Magnetic field profiles and electron phase space plots (x,γ) for $(b-a)/(c/\omega_{pe})=100$ (left panels) and for $(b-a)/(c/\omega_{pe})=500$. Here, unlike the previous simulations, the plasma density is constant in the upstream region. However, electron acceleration is also observed.

$$\frac{E_{\mathrm{II}}}{B_{\mathrm{II}}}=\frac{\int_{\mathrm{B}}^{\mathrm{C}}E_{\mathrm{II}}dt}{\int_{\mathrm{B}}^{\mathrm{C}}B_{\mathrm{II}}dt}. \tag{20}$$

The difference between the theoretical and observed values is small; i.e., 6%.

The initial electron temperature in this simulation was determined from the requirement for the numerical stability that the Debye length must be comparable to or greater than the grid spacing Δ_g;[35,36] thus, thermal velocity was $v_{T_e}/(\omega_{pe}\Delta_g)=1$. To see the effect of the electron temperature, we have carried out another simulation with $v_{T_e}/(\omega_{pe}\Delta_g)=0.5$, with the external magnetic field strength unchanged; hence, $v_{\mathrm{ms}}/(\omega_{pe}\Delta_g)=0.18$, which is 75% of the v_{ms} in the above simulation. It was then confirmed that the behavior of shock waves and accelerated electrons is essentially the same as that in the above simulation; that is, we have observed the formation of a secondary shock wave, generation of compressive and field-reversed pulses, and production of ultrarelativistic electrons due to these pulses. At $\omega_{pe}t=3250$, the maximum value of γ near the compressive pulses was ~ 60 and that near the field-reversed pulse was ~ 50 (the observed speeds of the original and secondary shock waves were $v_{\mathrm{sh}}=17.7v_{\mathrm{ms}}$ and $v_{\mathrm{sh}}=17.8v_{\mathrm{ms}}$, respectively).

C. Different inhomegeneity lengths and initial profiles

In this section, we examine the two acceleration processes in different inhomogeneity lengths $(b-a)$ and in different initial profiles.

Figure 10 shows electron phase space plots (x,γ) and profiles of B_z of simulations with a shorter inhomogeneity length, $(b-a)/(c/\omega_{pe})=100$ (left panels), and with a longer one, $(b-a)/(c/\omega_{pe})=500$ (right panels). In the left panels, high-energy electrons are found near compressive small pulses, such as the one at $x/(c/\omega_{pe})=2710$, and around the field-reversed pulse at $x/(c/\omega_{pe})=2680$. Here, the original shock wave has been damped out by this time. The speed of the secondary shock wave, the front of which is at $x/(c/\omega_{pe})=2830$ at this moment, is $v_{\mathrm{sh}}=13.4v_{\mathrm{ms}}$. The speed of the compressive pulse at $x/(c/\omega_{pe})=2710$ is $v_{\mathrm{cp}}=11.2v_{\mathrm{ms}}$, and that of the field-reversed pulse is $v_{\mathrm{np}}=11.3v_{\mathrm{ms}}$. In the right panels, high-energy electrons are produced mostly around compressive pulses; the acceleration is particularly strong behind the points $x/(c/\omega_{pe})=3265$ and $x/(c/\omega_{pe})=3272$. Their speeds are approximately $11v_{\mathrm{ms}}$. Here, the front of the secondary shock wave is at $x/(c/\omega_{pe})=3410$, propagating with a speed $14.2v_{\mathrm{ms}}$, while the original shock wave has been damped.

We show another different case in which the initial plasma density is constant, while the external magnetic field B_{z0} varies linearly as

$$B_{z0}(x)=B_{z0}(a)\left(1-\frac{2(x-a)}{b-a}\right), \tag{21}$$

in the region $a<x<b$. Strictly speaking, this does not satisfy the equilibrium condition (17). In the absence of shock waves, however, the profiles of B_z and n_i do not change much at least until $\omega_{pe}t=4000$, which is much longer than the time period in which a shock wave passes through the inhomogeneous region. In fact, the variance of B_z is quite small; for $(b-a)/(c/\omega_{pe})=500$,

$$\frac{1}{(b-a)B_{z0}(a)^2}\int_a^b[B_z(x)-B_{z0}(x)]^2dx=2.7\times10^{-4}, \tag{22}$$

at $\omega_{pe}t=4000$. In addition, that of n_i is 2.7×10^{-2}.

As in the above simulations, if a shock wave penetrates the inhomogeneous region, then a secondary shock wave is excited, and the two types of acceleration processes can occur. Figure 11 shows phase space plots (x,γ) and B_z profiles for the cases $(b-a)/(c/\omega_{pe})=100$ (left panels) and $(b-a)/(c/\omega_{pe})=500$ (right panels). In the former, electrons with $\gamma\simeq 90$ are present around the magnetic null point at $x/(c/\omega_{pe})=2590$. Here, the speed of this point is $v_{\mathrm{np}}=11.4v_{\mathrm{ms}}$, while that of the secondary shock at $x/(c/\omega_{pe})=2790$ is $v_{\mathrm{sh}}=13.5v_{\mathrm{ms}}$. In this case, the acceleration is predominant around the field-reversed pulse. Many electrons are, however, also energized around some compressive pulses. For instance, electrons near $x/(c/\omega_{pe})=2640$ gained energy around the time $\omega_{pe}t\sim 2000$; the compressive small pulse that caused the energization has disappeared by this time. The figures in the right panels are quite similar to those in the right panels of Fig. 10. The acceleration near the field-reversed pulse at $x/(c/\omega_{pe})=3205$ is insignificant, while many high-energy electrons are present behind the compres-

sive pulse at $x/(c/\omega_{pe})=3290$. The speed of this small pulse is $v_{cp}=11.9v_{ms}$, and that of the secondary shock wave at $x/(c/\omega_{pe})=3420$ is $v_{sh}=13.9v_{ms}$.

Compressive pulses produce a greater number of high-energy electrons than field-reversed pulses in many cases, particularly when $(b-a)$ is large. We compare the numbers of high-energy electrons averaged over the time $1000<\omega_{pe}t'<1500$, where t' is the time after the original shock wave has passed the right edge of the nonuniform region, $x=b$. The ratio of the number of electrons with $\gamma>25$ around the field-reversed pulse (n_{fr}) to that behind the compressive pulse (n_{cp}) is then about 0.25 for Fig. 7. Theses ratios n_{fr}/n_{cp} are 0.2 and 0.11, respectively, for the left and right panels in Fig. 10 and are 4.5 and 0.06, respectively, for the left and right panels in Fig. 11. In the present simulation parameters, the ratio n_{fr}/n_{cp} is larger when $(b-a)/(c/\omega_{pe})\sim 100$ than when $(b-a)/(c/\omega_{pe})\sim 500$. The left panel of Fig. 11 is the only case in which n_{fr}/n_{cp} exceeds unity.

We have also tested the cases in which there is no field reversal; i.e., $B_{z0}(x)>0$ at any points. In such circumstances, compressive small pulses are also newly generated after the original shock wave has passed through the inhomogeneous region. The electron energy accelerated by theses pulses was low compared with those in the above cases. For instance, for a stepwise external magnetic field such that $B_{z0}(x)=B_{z0}(a)$ for $x\leq a$ and $B_{z0}(x)=B_{z0}(a)/2$ for $x>a$, electron energies accelerated by these pulses were $\gamma\lesssim 20$.

IV. SUMMARY

By using a relativistic particle simulation code, we have studied the effect of inhomogeneity of background plasmas on shock propagation and electron acceleration, with particular attention to the generation of field profiles that can accelerate electrons after the original shock wave enters the inhomogeneous region. Specifically, we have considered shock waves in an external magnetic field B_{z0} that varies with x in a finite region $a<x<b$ from $B_{z0}(a)(>0)$ to $B_{z0}(b)=-B_{z0}(a)$ and examined several cases, with different inhomogeneity lengths $(b-a)$ and with different initial profiles of B_{z0} and n_i. The field strength was taken to be $|\Omega_e|/\omega_{pe}=0.4$ in the far upstream region.

Simulations under these conditions show that before a shock wave with positive B_z reaches the point $x=a$, some electrons are accelerated by a compressive small pulse; this is the same mechanism as the one described in Ref. 12. After penetrating the inhomogeneous region, the original shock wave is damped in the reversed field. A secondary shock wave with negative B_z is then excited in the region $x>b$. In this wave, some electrons are accelerated to ultrarelativistic energies immediately behind newly generated compressive small pulses. Further, energization around a field-reversed pulse is also found. Since these pulses are under the influence of the shock wave, electric fields exist around them; electrons can absorb energy from them. These simulations indicate that the inhomogeneity enhances the generation of particle-accelerating small pulses.

Electron acceleration due to compressive and field-reversed pulses in large-amplitude magnetosonic waves can occur in solar flares. Since the fields in coronal magnetic tubes are quite strong, i.e., $B\lesssim 10^3$ G, the electron acceleration mechanism discussed in Ref. 11 can also operate in solar flares. (For $B=10^2$ G and $n=10^8$ cm^{-3}, we have $|\Omega_e|/\omega_{pe}\simeq 3$.) When the fields are weak, i.e., $|\Omega_e|<\omega_{pe}$, the present mechanisms would be more important.

The interaction between shock waves and striped pulsar wind would be another attractive theme to which the present study could be applied. It is suggested[29,30] that toroidal stripes of opposite magnetic polarity are formed in the wind emanating from an obliquely rotating pulsar. Lyubarsky[31] then discussed the driven reconnection of alternating fields due to the termination shock as a possible dissipation mechanism of the wind energy. The extension of the present analysis to the case of alternating fields is of considerable interest.

In the present paper, simulations were focused on perpendicular shock waves, even though the acceleration theory (10) should be applicable to oblique cases. Evolution of oblique shock waves in a nonuniform external magnetic field and electron acceleration due to field-reversed and compressive small pulses will be discussed elsewhere. Another important effect that should be examined is the magnetic reconnection, which could occur in field-reversed configurations. Its study requires two- or three-dimensional analysis. In the future, it is desirable to investigate the present acceleration processes with multidimensional, relativistic particle simulations.

ACKNOWLEDGMENTS

This work was carried out by the joint research program of the Solar-Terrestrial Environment Laboratory, Nagoya University, and by the collaboration program, NIFS04KTAT003, of the National Institute for Fusion Science.

[1] D. J. Forrest and E. L. Chupp, Nature (London) **305**, 291 (1983).
[2] H. Nakajima, T. Kosugi, K. Kai, and S. Enome, Nature (London) **305**, 292 (1983).
[3] S. R. Kane, E. L. Chupp, D. J. Forrest, G. H. Share, and E. Rieger, Astrophys. J. Lett. **300**, L95 (1986).
[4] T. Tanimori, K. Sakurazawa, S. A. Dazeley *et al.*, Astrophys. J. Lett. **492**, L33 (1998).
[5] F. A. Aharonian, A. G. Akhperjanian, J. A. Barrio *et al.*, Astrophys. J. **539**, 317 (2000).
[6] K. Koyama, R. Petre, E. V. Gotthelf *et al.*, Nature (London) **378**, 255 (1995).
[7] T. Tanimori, Y. Hayami, S. Kamei *et al.*, Astrophys. J. Lett. **497**, L25 (1998).
[8] T. Tajima and J. M. Dawson, Phys. Rev. Lett. **43**, 267 (1979).
[9] C. Joshi and T. Katsouleas, Phys. Today **56**(6), 47 (2003).
[10] V. Malka, S. Fritzler, E. Lefebvre *et al.*, Science **298**, 1596 (2002).
[11] N. Bessho and Y. Ohsawa, Phys. Plasmas **6**, 3076 (1999); **9**, 979 (2002).
[12] M. Sato, S. Miyahara, and Y. Ohsawa, Phys. Plasmas **12**, 052308 (2005).
[13] B. Lembege and P. Savoini, Phys. Fluids B **4**, 3533 (1992).
[14] T. Kawashima, S. Miyahara, and Y. Ohsawa, J. Phys. Soc. Jpn. **72**, 1664 (2003).
[15] J. H. Adlam and J. E. Allen, Philos. Mag., Suppl. **3**, 448 (1958).
[16] L. Davis, R. Lüst, and A. Schlüter, Z. Naturforsch. A **13**, 916 (1958).
[17] Y. Ohsawa, Phys. Fluids **29**, 1844 (1986); **29**, 2474 (1986).
[18] C. S. Gardner and G. K. Morikawa, Commun. Pure Appl. Math. **18**, 35 (1965).
[19] T. Kakutani, H. Ono, T. Taniuti, and C. C. Wei, J. Phys. Soc. Jpn. **24**, 1159 (1968).
[20] C. S. Morawetz, Phys. Fluids **4**, 988 (1961).

[21]D. Biskamp and H. Welter, Nucl. Fusion **12**, 663 (1972).
[22]C. F. Kennel and R. Pellat, J. Plasma Phys. **15**, 335 (1976).
[23]D. W. Forslund, K. B. Quest, J. U. Brackbill, and K. Lee, J. Geophys. Res., [Oceans] **89**, 2142 (1984).
[24]Y. Ohsawa, Phys. Fluids **28**, 2130 (1985); Y. Ohsawa, J. Phys. Soc. Jpn. **59**, 2782 (1990).
[25]B. Lembege and J. M. Dawson, Phys. Fluids B **1**, 1001 (1989).
[26]R. L. Tokar, S. P. Gary, and K. B. Quest, Phys. Fluids **30**, 2569 (1987).
[27]E. G. Harris, Nuovo Cimento **23**, 115 (1962).
[28]D. Biskamp, *Magnetic Reconnection in Plasmas* (Cambridge University Press, Cambridge, 2000), Chap. 7.
[29]F. C. Michel, Comments Astrophys. Space Phys. **3**, 80 (1971).
[30]F. V. Coroniti, Astrophys. J. **349**, 538 (1990).
[31]Y. E. Lyubarsky, Mon. Not. R. Astron. Soc. **345**, 153 (2003).
[32]V. S. Imshennik and S. I. Syrovatskii, Sov. Phys. JETP **52**, 990 (1967).
[33]J.-I. Sakai, T. Tajima, and F. Brunel, Sol. Phys. **91**, 103 (1984).
[34]P. C. Liewer, A. T. Lin, J. M. Dawson, and M. Z. Caponi, Phys. Fluids **24**, 1364 (1981).
[35]A. B. Langdon, J. Comput. Phys. **6**, 247 (1970).
[36]H. Okuda, J. Comput. Phys. **10**, 475 (1972).